GLOBAL SCIENTIFIC INC.

ORIGINAL ARTICLE

Catalytic performance and kinetics study of titania-supported catalysts in NH₃-SCR process

Denghui Wang*, Shien Hui, Shuai Wang, Sheng Liu

School of Energy and Power Engineering, Xi'an Jiaotong University, Xi'an 710049, (CHINA)
E-mail: denghuiwang@163.com

Abstract : NH₃-based selective catalytic reduction (SCR) technology has been widely applied to reduce the pollution resulted from NOx. In this study, the catalytic activity of two different titania-supported catalysts was tested in a self-designed lab-scale experimental system. Moreover, the differences between them were compared for further analysis with the help of advanced characterization techniques such as X-ray fluorescence (XRF), inductively coupled plasma-optical emission spectroscopy (ICP-OES), N_2 adsorption-desorption with BET method, and X-ray diffraction (XRD). The catalytic efficiency of the two catalysts increased as either the residence time or the reaction temperature rose, while catalyst B performed better than catalyst A at similar conditions. Finally, the activation energy and frequency factor of the reaction over each catalyst were investigated and calculated in this study, and our results indicated that the reaction activation energy of catalyst A was higher than that of catalyst B, but the frequency factor was lower.
© **Global Scientific Inc.**

INTRODUCTION

As the increasing combustion of fossil fuels all over the world, NOx (NO and NO_2) emission has been a more and more seriously environmental problem for decades[1], because it easily results in photochemical smog, acid rain, greenhouse effect, and fine particulates[2,3]. In the exhausts from combustion facilities, more than 95% of NOx is NO and the other 5% is NO_2. To reduce the pollution resulted from NOx, NH₃-based selective catalytic reduction (SCR) technology has been widely used in power plants, waste incinerators, and gas turbines[4]. In the SCR process, titania-supported catalysts are most commonly used[5,6], so the DeNOx performance of catalysts becomes the most concerned part for engineers and researchers.

In recent years, much attention has been focused on the development of highly efficient catalysts[7-10], and the effect of physio-chemical properties on the DeNOx activity has also been widely discussed[11-14]. Seunghee Youn *et al.*[15] investigated the effect of vanadium precursor solution with different oxidation states on the NH₃-SCR reaction and physio-

ORIGINAL ARTICLE

chemical properties of V_2O_5/TiO_2 catalysts, and it was found that the physio-chemical properties of vanadia species can be changed as a function of oxidation state of vanadium precursor solution. Dong Wook Kwon et al.[16] prepared the catalyst by synthesizing V_2O_5 and anatase TiO_2 with the mechanochemical method, and the NH_3-SCR reactive properties were studied by using physio-chemical analysis to explore the causes for the increased activity and reactive characteristics of the crystal and surface structures of the catalyst. Song Zhou et al.[17] developed a SCR catalyst testing system and studied the catalytic activities of an extruded commercial monolithic V_2O_5-WO_3/TiO_2 catalyst at low temperatures.

Although much research has been devoted to the preparation and performance analysis of titania-supported catalysts, little attention has been paid to the activation energy and the frequency factor of NH_3-SCR reaction over commercial titania-supported catalysts. In the experiments reported here, we tested the DeNOx activity of two different SCR catalysts used in power plants and compared the differences between them with the help of advanced characterization techniques for further analysis. Moreover, the activation energy and the frequency factor of the reaction over each catalyst were investigated and calculated in this study.

EXPERIMENTAL

Experimental setup

Figure 1 illustrates the experimental setup used in this study. Primary composition of the flue gas was supplied by cylinders containing NO/N_2, NH_3/N_2, O_2, and N_2. The relative parameters of the cylinder gas are given in TABLE 1. The gas flow rate is controlled by mass flowmeter, and mass flowmeter was corrected by soap film flowmeter. The exhausted gas after DeNO$_x$ reaction flew into a gas analyzer through a polytetrafluoroethylene pipe, which was heated to 105°C. The flue gas analyzer (GASMET FTIR Dx4000) measures the concentrations of gases (NO, NO_2, N_2O, NH_3, etc.) to be as low as 0.2 ppm, and the measurement accuracy is ±2%.

The flow rate of the total gas was kept 1L/min (STP, the same below), which contains 4% O_2, 24 mmol/L NH_3 and 24 mmol/L NO with the balance N_2.

Catalyst characterization

The element contents of catalysts were measured by X-ray fluorescence (XRF) spectrometer (Bruker AXS GmbH, S4 PIONEER). The measurement range of the XRF spectrometer is from 0.5 ppm to 100% with the measurement accuracy of 0.05%, and the
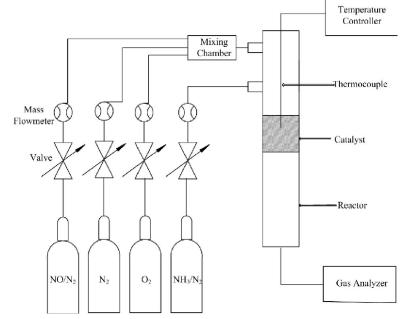

Figure 1 : Experimental setup

ORIGINAL ARTICLE

Gas	Purity	Gas	Molar Ratio
N_2	99.999%	NO/N_2	5%
O_2	99.99%	NH_3/N_2	5%

comprehensive long-term stability is better than 0.05%. The angle repeatability is less than ±0.0001°, and the measurement time for each element is 10 to 30 seconds.

The inductively coupled plasma-optical emission spectroscopy (ICP-OES) (Perkin Elmer, Optima 8000) was used to analyze the vanadium content in catalysts. The Optima 8000, adopting Flat Plate plasma technology, is a bench-top, dual-view ICP-OES with full-wavelength-range charge coupled device (CCD) array detector. The preparation method of the standard solution and the test solution was as follows: a 44.64 mmol/m³ vanadium standard solution was separately diluted by 1000 times and 250 times to 0.04464 mmol/m³ and 0.1786 mmol/m³ vanadium standard solutions; the catalyst samples about 0.5 g were added into a mixture of 20 ml HNO_3 and 5 ml HF, and then the solution was heated in order to dissolve the catalyst samples and was set volume to 200 ml, after which it was diluted by 10 times and filtered by 0.25 μm filter membrane to finish the samples to be tested. Cross Flow configuration was adopted during the test process.

The BET (Brunauer-Emmett-Teller) surface area and the pore structures of catalysts were measured from N_2 adsorption and desorption isotherms using the AutoChem II 2920 (Micromeritics) fully automated chemisorption analyzer. In this research, the specific surface area was calculated by BET method, while the pore diameter and the pore volume were calculated by BJH (Barrett-Joyner-Halenda) method.

The crystalline morphology and grain size of the catalysts were studied using X-ray diffraction (XRD). Full XRD patterns were taken with X'pert Pro (PANalytical) operated at 40 KV and 30 mA. The catalysts were run 2θ ranging from 10° to 90° with step size 0.033°.

Catalytic activity measurement

In this paper, the catalytic activity of powder catalysts in the DeNOx process was measured by comparing the different content of NO before and after the reaction process.

NO reduction efficiency X is defined as:

$$X = \frac{C_{NO}^{in} - C_{NO}^{out}}{C_{NO}^{in}} \times 100\% \tag{1}$$

where C_{NO}^{in} and C_{NO}^{out} respectively refer to the NO concentrations at the entrance and exit of the experimental setup in a experiment condition.

RESULTS AND DISCUSSION

Component analysis of catalysts

Two different types of catalysts, named catalyst A and catalyst B in this research, were tested for analyzing the related causes for DeNOx efficiency differences and further exploring the activation energy of the DeNOx reaction. The catalysts were commercial catalysts, and both of them were prepared by the sulfuric acid method.

The element analysis result of catalysts is listed in TABLE 2, and in both catalysts elements Ti, W, O, and Si were over 1 wt.%, but elements Ca, S, and Ba in catalyst B were also relatively more than others. There were much more Ti and V in catalyst A than those in catalyst B, while the content of W and Ba was less. As is known to researchers, Ti and V play a vital role in DeNOx reaction[18-20], while W and Ba also has positive effect on the $DeNO_x$ efficiency[21-23]. According to the vanadium content in catalysts, it could be calculated that the V_2O_5 content in catalyst A and B was separately 0.75% and 0.55%. There was more SO_4^{2-} in catalyst B than that in catalyst A, and it was in the state of free sulphate and $BaSO_4$ existing in catalyst B, while there was little $BaSO_4$ in catalyst A.

After the low temperature calcination process, DeNOx catalysts are mainly composed of TiO_2, WO_3, SiO_2, V_2O_5, and other oxides, so it is also necessary to confirm the catalyst component by oxide analysis. As shown in TABLE 3, the oxide contents

TABLE 2 : Element analysis of catalysts

Element	Ti	O	W	Si	Ca	S	V	Al	Fe
A (wt.%)	63.90	26.60	5.71	1.28	0.91	0.58	0.42	0.37	0.05
B (wt.%)	54.50	27.75	6.93	1.83	1.80	1.46	0.31	0.61	0.09

Element	Zr	Ba	Na	Mg	Nb
A (wt.%)	0.04	0.03	0.03	0.01	—
B (wt.%)	0.10	4.55	0.03	0.06	0.08

TABLE 3 : Oxide analysis of catalysts

Oxide	TiO_2	WO_3	BaO	SiO_2	CaO	SO_3	Al_2O_3	V_2O_5	Fe_2O_3
A(wt.%)	87.1	6.6	0.08	2.42	1.06	1.24	0.64	0.61	0.06
B(wt.%)	78.9	6.67	3.98	3.5	2.17	3.2	1.03	0.30	0.11

Oxide	ZrO_2	Nb_2O_5	Na_2O	K_2O	P_2O_5
A(wt.%)	0.05	0.05	0.03	0.01	0.05
B(wt.%)	0.13	—	—	0.03	0.06

in both catalysts are listed, and it could be seen that V_2O_5 in catalyst A and B was separately 0.61% and 0.30%, which was a little different from the results calculated from TABLE 2.

XRF is actually a semi-quantitative analysis method, and it is easily influenced by superposition and disturbance of element peaks. In DeNO*x* catalysts, the active ingredient vanadium performs the greatest efficiency and has important influence on the catalyst activity and selectivity, so it is quite necessary to measure and confirm the vanadium content by a quantitative analysis method. In this research, the ICP-OES was applied to finish the measurement of vanadium in catalysts. The results are listed in TABLE 4, and we adopt these results as the real vanadium content.

BET surface area, BJH pore diameter and BJH pore volume

Physical properties of a catalyst, such as BET surface area, BJH average pore diameter and BJH total pore volume, are very important to determine the adsorption-desorption phenomena of gases onto its surface[24]. TABLE 5 compares these physical measures for catalyst A and catalyst B. The BET surface area of catalyst A was much more than that of catalyst B, but the total pore volume of the two catalysts were similar, which led to a smaller average pore diameter of catalyst A.

XRD studies

Figure 2 illustrates the XRD patterns of two catalysts, while the diffraction peak position and the peak intensity of TiO_2, $BaSO_4$, VO_2 and V_2O_5 are illustrated on the lower part of Figure 2. The peaks corresponding to anatase TiO_2 phase could be detected obviously and the peaks shaped sharp. From the enlarged view of the TiO_2 (101) diffraction peak it could be found that the diffraction peak of catalyst B was weaker than that of catalyst A. Catalyst B exhibited characteristic $BaSO_4$ peaks, while catalyst A did not. Furthermore, no V_2O_5 peak or VO_2 peak

TABLE 4 : Vanadium content in catalysts

Catalyst	A	B
V (wt.%)	0.37	0.33
V_2O_5 (wt.%)	0.66	0.59

TABLE 5 : Physical properties of catalysts

Sample	BET surface area (m^2/g)	Average pore diameter (nm)	Total pore volume (0.85 to 150nm, cm^3/g)
A	66.8	13.4	0.279
B	54.6	16.4	0.274

ORIGINAL ARTICLE

Figure 2 : XRD patterns of catalysts

TABLE 6 : Residence time of different amounts of catalysts

Catalyst mass (g)	0.10	0.15	0.20	0.25	0.30	0.40	0.50
Residence time for A (s)	0.0082	0.0124	0.0165	0.0206	0.0247	0.0330	0.0412
Residence time for B (s)	0.0074	0.0112	0.0149	0.0186	0.0223	0.0298	0.0372

could be observed in either of the two catalysts, which suggested that the vanadium oxides did not form large grain structures and they loaded onto the surface of TiO_2 carrier in a highly dispersed state. We calculated the grain sizes of catalysts perpendicular to the 101 crystal face and the 200 crystal face according to the Scherrer formula, and we averaged the sizes of two crystal faces as the final result. The grain sizes of catalyst A and B were separately 20.3 nm and 19.2 nm.

DeNO*x* efficiency of catalysts

By use of mercury intrusion method, the bulk density of catalyst A and catalyst B, both in the form of 40 to 65 mesh particles, was separately measured 0.6980 g/ml and 0.7608 g/ml under the mercury injection pressure of 1724 Pa. Moreover, by use of microgram balance weighing method, the tap density of catalyst A and B was separately measured 0.7273 g/ml and 0.8058 g/ml. During the experiments in this research, catalysts were sandwiched tightly between two layers of mullite asbestos, so it was more appropriate to utilize the tap density for calculating the residence time.

The internal diameter of the reactor designed for powder catalysts was 7 mm, and the total gas flow during the experiments was 1 L/min, so the residence time of different amounts of catalysts could be calculated according to the tap density and the above data, as shown in TABLE 6.
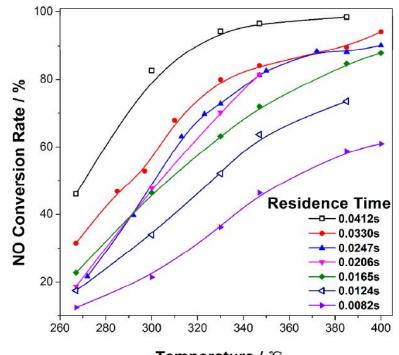
'The DeNO*x* efficiency of catalysts measured in different residence time and different reaction temperature was as shown in Figure 3 and Figure 4, from which we could see that the DeNO*x* efficiency increased gradually as the residence time rose. Moreover, when the reaction temperature rose, the efficiency of both catalyst A and catalyst B increased significantly. Tested in similar residence time, catalyst B performed greater efficiency than catalyst A.

DeNO*x* reaction rate equation of catalysts

The equation of the intrinsic chemical reaction rate and the reactant concentration in gas phase is as follows:

$$r_{NO} = k_c C_{NO}^{\alpha} C_{NH_3}^{\beta} C_{O_2}^{\gamma} C_{H_2O}^{\delta} \tag{2}$$

where r_{NO} is the chemical reaction rate represented by the NO concentration variation, k_c is the reac-

Figure 3 : NO conversion rate of catalyst A under different residence time and different reaction temperature
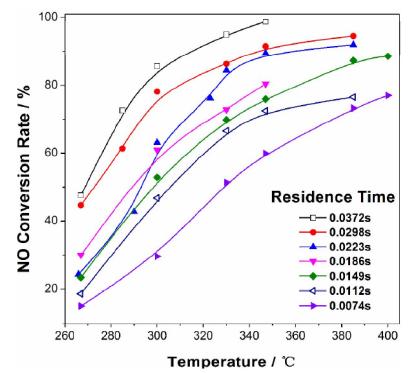

Figure 4 : NO conversion rate of catalyst B under different residence time and different reaction temperature

tion rate constant, and C is the reactant concentration.

If the molar ratio of n(NH$_3$)/n(NO) is higher than or equal to 1.0, $\beta = 0$. If the concentration of O$_2$ is more than 2%, the effect of γ on r_{NO} can be ignored.

Considering there is not H$_2$O in the experiments, Eq.2 can be written in the simplified form[25,26]:

$$r_{V\_NO} = k_{V\_NO}C_{NO} = k_{V\_NO}C_{NO}^{in}(1-X) \qquad (3)$$

where r_{V_NO} is the reaction rate expressed by the

ORIGINAL ARTICLE

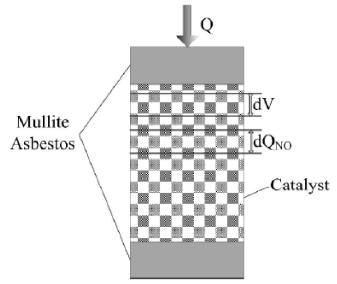**Figure 5 : Illustration for DeNOx reaction model**

The NO conversion rate in the whole DeNO*x* process is X, and the rate in volume is , so can be represented as

$$dX = \frac{C_{NO}^{dV_{in}} - C_{NO}^{dV_{out}}}{C_{NO}^{dV_{in}}} \times 100\% \qquad (4)$$

where $C_{NO}^{dV_{in}}$ is the inlet NO volume fraction of the dV volume, and $C_{NO}^{dV_{out}}$ is the outlet NO volume fraction of the dV volume.

The relationship of dX, dQ_{NO} and Q_{NO} is

$$dQ_{NO} = Q_{NO}dX \qquad (5)$$

The material balance equation of NO in dV volume is
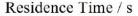
$$Q_{NO}dX = r_{V\_NO}dV \qquad (6)$$

Figure 6 : Reaction rate constant k_{V_NO} of catalyst A for different temperature

variation of volume fraction, C_{NO}^{in} is the inlet volume fraction of NO, X is the conversion rate of NO, and k_{V_NO} is the reaction rate constant.

The reduced DeNO*x* reaction model[27-29] is as shown in Figure 5, while the total catalyst volume and the total gas flow is respectively marked as V and Q. In the inlet gas, the NO volume is Q_{NO}, and the NO volume reduces dQ_{NO} after dV catalyst.
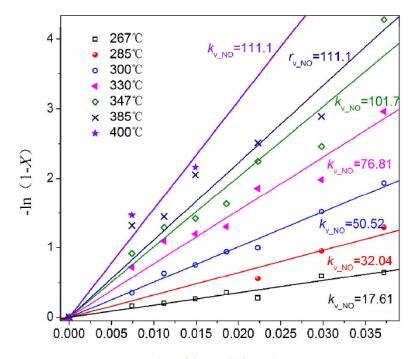
Considering Eq.3, we obtain

$$k_{V\_NO}C_{NO}^{in}(1-X)dV = Q_{NO}dX = QC_{NO}^{in}dX \qquad (7)$$

Upon performing the integration of the whole volume V, we obtain

$$k_{V\_NO}\frac{V}{Q} = -\ln(1-X) \qquad (8)$$

For $\tau = V/Q$, Eq.8 takes the form

$$k_{V\_NO}\tau = -\ln(1-X) \qquad (9)$$

Figure 7 : Reaction rate constant k_{V_NO} of catalyst B for different temperature
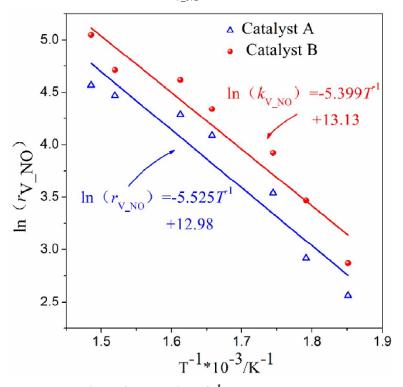

Figure 8 : Equation of k_{V_NO} ln and T^{-1}

According to the relationship between the residence time and the DeNOx efficiency, we could achieve the variation of the DeNOx efficiency with the residence time, as shown in Figure 6 and Figure 7. From the experimental data in Figure 3 and Figure 4, we could gain different reaction rate constant k_{V_NO} for different reaction temperature.

According to the Arrhenius law, the relationship between k_{V_NO} and T is as follows:

ORIGINAL ARTICLE

TABLE 7 : Calculated results of activation energy and frequency factor

Catalyst	Activation energy (kJ/mol)	Frequency factor (s⁻¹)
A	45.93	4.339*10^5
B	44.88	5.058*10^5

$$\ln k_{V\_NO} = -\frac{E}{RT} + \ln k_{0V\_NO} \qquad (10)$$

where k_{0V_NO} is the frequency factor, and E is the reaction activation energy.

From Figure 6 and Figure 7, the different k_{V_NO} for different reaction temperature could be clearly calculated, so the relationship of $\ln k_{V\_NO}$ and T^{-1} can be expressed linearly in Figure 8.

The reaction activation energy can be obtained from the linear intercept in Figure 8, and the frequency factor can be obtained from the linear slope in Figure 8. The calculated results are listed in TABLE 7, from which we could see that the reaction activation energy of catalyst A was higher than that of catalyst B, but the frequency factor was lower. The higher activation energy accounted for the higher light-off temperature of DeNOx reaction, and the lower frequency factor accounted for the lower effective collision frequency of reactant molecules and active sites, so catalyst A performed lower DeNOx activity than catalyst B.

According to the results in TABLE 7, Eq.3 could be written as Eq.11 and Eq.12 for catalyst A and catalyst B:

$$r_{V\_NO} = 4.339 \times 10^5 \exp\left(\frac{45930}{8.314 \times T}\right) C_{NO}^{in}(1-X) \quad (11)$$

$$r_{V\_NO} = 5.058 \times 10^5 \exp\left(\frac{44880}{8.314 \times T}\right) C_{NO}^{in}(1-X) \quad (12)$$

CONCLUSIONS

The catalytic activity of two different titania-supported NH$_3$-SCR catalysts was tested in a self-designed lab-scale experimental system, and various analytical techniques were utilized to explore the physico-chemical properties of catalysts and the causes for the DeNOx differences between them. The BET surface area of catalyst A was higher than that of catalyst B, but the similar total pore volume of the two catalysts led to a smaller average pore diameter of catalyst A. On XRD patterns, the two catalysts exhibited characteristic TiO$_2$-anatase peaks but not TiO$_2$-rutile peaks. However, no peak assigned to V$_2$O$_5$ or VO$_2$ was observed, implying that the vanadium oxides were well dispersed on the surface of TiO$_2$ carrier. An increase in the residence time or in the reaction temperature could result in an increase in the catalytic efficiency of both the two catalysts, and catalyst B performed higher efficiency than catalyst A at similar reaction conditions. Through the calculated results, it could be concluded that the reaction activation energy of catalyst A was higher than that of catalyst B, but the frequency factor was lower. Therefore, the higher light-off temperature of the DeNOx reaction and the lower effective collision frequency of reactant molecules and active sites resulted in the lower catalytic activity of catalyst A.

REFERENCES

[1] K.Skalska, J.S.Miller, S.Ledakowicz; *Sci.Total Environ.,* **408**, 3976 (**2010**).

[2] S.Lee, K.Park, J.W.Park, B.H.Kim; *Combust.Flame,* **141**, 200 (**2005**).

[3] S.Niu, K.Han, C.Lu; *Process Saf.Environ.,* **89**, 121 (**2011**).

[4] S.Eswaran, H.G.Stenger; *Fuel Process.Technol.*, **89**, 1153 (**2008**).

[5] L.J.Alemany, F.Berti, G.Busca; *Appl.Catal.B,* **10**, 299 (**1996**).

[6] H.Bosch, F.Janssen; *Catal.Today* 2 v, (**1988**).

[7] F.Chiker, J.P.Nogier, J.L.Bonardet; *Catal.Today,* **78**, 139 (**2003**).

[8] S.Zhang, Q.Zhong; *J.Mol.Catal.A: Chem.,* **373**, 108 (**2013**).

[9] H.F.Huang, L.L.Jin, H.F.Lu, H.Yu, Y.J.Chen; *Catal.Commun.*, **34**, 1 (**2013**).

[10] R.Xue, C.Chen, Q.Wang, M.Zhou, S.Chen; *Asian J.Chem.,* **26**, 1667 (**2014**).

[11] J.Arfaoui, L.K.Boudali, A.Ghorbel, G.Delahay; *Catal.Today,* **142**, 234 (**2009**).

[12] I.E.Wachs, B.M.Weckhuysen; *Appl.Catal.A,* **67**, 1-2, (**1997**).

[13] F.Tang, K.Zhuang, F.Yang, L.Yang, B.Xu, J.Qiu, Y.Fan; *Chinese J.Catal.,* **933**, 4-6 **(2012)**.

[14] J.Xie, Z.Fu, F.He, J.Chen, D.Fang, Y.Zhang; *Asian J.Chem.,* **25**, 4416 **(2013)**.

[15] S.Youn, S.Jeong, D.H.Kim; *Catal.Today,* **232** 185 **(2014)**.

[16] D.K.Kwon, K.H.Park, S.C.Hong; *Appl.Catal.A*, **451**, 227 **(2013)**.

[17] S.Zhou, Y.Liu, Y.Q.Zhu, Y.Yu, C.L.Li; *Asian J.Chem.,* **14**, 8075 **(2013)**.

[18] G.L.Bauerle, S.C.Wu, K.Nobe; *Ind.Eng.Chem.Prod.Res.Dev.*, **17**, 117 **(1978)**.

[19] F.Nakajima, I.Hamada; *Catal.Today,* **29**, 109 **(1996)**.

[20] V.I.Pârvulescu, P.Grange, B.Delmon; *Catal.Today,* **46**, 233 **(1998)**.

[21] M.Kobayashi, K.Miyoshi; *Appl.Catal.B,* **72**, 253 **(2007)**.

[22] H.Bosch, F.Janssen; *Catal.Today,* **2**, 403 **(1988)**.

[23] J.W.Chounga, I.S.Nama, S.W.Hamb; *Catal.Today,* **242**, 3-4 **(2006)**.

[24] M.S.Maqbool, A.K.Pullur, H.P.Ha; *Appl.Catal.B,* **28**, 152-153 **(2014)**.

[25] N.Y.Topsoe, J.A.Dumesic, H.Topsoe; *J.Catal,* **151**, 241 **(1995)**.

[26] G.Busca, L.Lietti, G.Ramis, F.Berti; *Appl.Catal.B,* **18**, 1 **(1998)**.

[27] S.R.Dhanushkodi, N.Mahinpey, M.Wilson; *Process Saf.Environ.,* **86** 303 **(2008)**.

[28] Mejia I.Centeno, S.Castillo, R.Camposeco, G.A.Fuentes; *Catal.Commun.,* **31**, 11 **(2013)**.

[29] M.D.Amiridis, J.P.Solar; *Ind.Eng.Chem.Res.*, **35**, 978 **(1996)**.